ELSEVIER

Journal of Chromatography A, 758 (1997) 175–190

JOURNAL OF CHROMATOGRAPHY A

Effect of column efficiency on the internal concentration profiles and the performance of a simulated moving-bed unit in the case of a linear isotherm

Tong Yun[a,c], Zouhir Bensetiti[b,c], Guoming Zhong[b,c], Georges Guiochon[b,c,*]

[a]*Department of Chemical Engineering, University of Tennessee, Knoxville, TN 37996-2200, USA*

[b]*Department of Chemistry, University of Tennessee, Knoxville, TN 37996-1600, USA*

[c]*Division of Chemical and Analytical Sciences, Oak Ridge National Laboratory, Oak Ridge, TN 37831-6120, USA*

Received 15 April 1996; revised 20 August 1996; accepted 20 August 1996

Abstract

Simulated moving-bed (SMB) separators have been used successfully to separate or purify continuously two components with different adsorption selectivities. A detailed understanding of their behavior is still lacking, however. A numerical solution of the equilibrium–dispersive model allows the calculation of the concentration profiles along the columns, of their progressive shifts during a cycle, of the progressive build-up of these concentration profiles in each column during the start-up period, of the concentration profiles under steady-state and of the concentration histories at the extract and raffinate ports. These profiles are illustrated and discussed. The results obtained are compared to those of the exact analytical solution of the linear, ideal model previously developed. This comparison illustrates the influence of column efficiency on the time needed to reach steady-state operation.

Keywords: Simulated moving-bed chromatography; Column efficiency; Concentration profiles

1. Introduction

Simulated moving-bed (SMB) is a powerful separation process that allows the continuous separation of large amounts of feedstocks into two streams of products. It was initially developed for the separation of *p*-xylene from a C_8-hydrocarbon fraction (Parex process [1,2]) and was successfully used for the separation of olefins and paraffins (Olex), of *n*-paraffins from branched and cyclic hydrocarbons (Molex [3]), of fructose from corn syrup hydrolyzates (Sarex) and of other compounds [2–5]. Later, the separations of glucose and fructose [6,7], of glucose and sodium chloride [8], of phenylalanine and sodium chloride [7], of α-cyclodextrin and glucose [9] and of glutathione and glutamic acid [10] were investigated. All of these applications have been carried out on a very large industrial scale. The total world production by all the Sorbex processes was 5 million ton per year in 1984 [5].

Compared to overloaded elution or, for that matter, to displacement chromatography, SMB has the major advantage of giving a 100% recovery yield and no mixed fractions to reprocess. The feed is pumped continuously into the column series, as well as the mobile phase (or desorber), while two streams

*Corresponding author. Address for correspondence: Department of Chemistry, University of Tennessee, Knoxville, TN 37996-1600, USA.

PII S0021-9673(96)00735-2

of products, the raffinate and the extract, are recovered continuously. The components entering with the feed must exit with one of the two products. The separation operation is carried out at high concentrations, which allows full use of the non-linear effects, and especially of the displacement effect, to enhance separation and production rate. Finally, a better use is made of the stationary phase in the columns. This phase is more often in quasi-equilibrium with a mobile phase containing a high concentration of the feed components than in the more conventional batch processes. Conversely, the main drawbacks of the SMB process are its greater complexity, from both the experimental and the conceptual standpoints, and the fact that an SMB can separate the feed into only two different fractions, one containing the more weakly retained components, the other the more strongly retained ones. Other significant drawbacks are the long start-up period and the high inventory of product stored in the SMB during a production campaign.

The SMB process is now attracting considerable interest as an alternative to the use of overloaded elution for the separation and purification of relatively small amounts of pharmaceuticals or pharmaceutical intermediates. The use of the SMB process for the purification of enantiomers appears particularly attractive, from both the technical and the economical points of view [11]. The new FDA regulations [12] consider the two enantiomers as different pharmaceuticals (unless they interconvert in body fluids within a few hours). Because it is a binary separation, the purification of an enantiomer is ideally suited for SMB, whether it uses, as feed, the racemic mixture or the insufficiently pure product of an enantioselective synthesis. Such synthesis are rarely selective enough to eliminate the need for a purification step. However, chiral phases exhibit usually low or moderate values of the separation factors (more often between 1.1 and 1.4 than larger than 2) and low values of the saturation capacity [13]. This results in more severe requirements for the performance of the SMB than the earlier, easier industrial separations previously reported [1–10] and more critical optimum conditions. The successful development of new applications in the pharmaceutical industry requires a better, more comprehensive understanding of the SMB process.

Several fundamental investigations of the SMB process have been published [14–18]. Various models have been developed to calculate the concentration profiles of two components along the different columns, constituting its four sections and the concentration histories at the two ports. Most of these studies used a linear or a non-competitive Langmuir isotherm. Either one of these models is a good approximation in the case of the separation of sugars, for example, because their equilibrium isotherms between an aqueous solution and the ion-exchange resins used to separate them are nearly linear and are either non-competitive or weakly competitive [17]. Although this assumption is no longer valid for enantiomeric mixtures, it is important, as a starting point, to have a good understanding of the mechanism of separation under linear conditions in an SMB unit.

The general principles of operation of the SMB are now well understood. However, there remains considerable uncertainty regarding almost all details of its design, method development and optimization for any new applications. Among the important issues that are still insufficiently well understood are the terms of the trade-offs between product purity and production rate. In other words, what is the cost, in terms of lost production rate, of an increase in the purity of the products by a few percentage points. This is an important practical question to which theory should provide an answer. Little is known also about the relationships between fraction purity, column efficiency and separation factor. Semi-empirical rules have been suggested recently, giving some interesting new insights [18]. Conventionally, the SMB process uses a series of columns divided into four sections. What are the advantages and inconveniences of using one, two, three or more columns per section? Is it even necessary to have the same number of columns in each section? What happens if the different columns have significantly different characteristics and performance; in particular, different efficiency, retention factors, separation factor, isotherm parameters and permeability? We know how difficult it is to pack columns that have values for these different characteristics that are very similar.

We have undergone a systematic study of these problems in an effort to clarify the main issues

involved in the development of new applications of the SMB process. In previous papers, we have presented an analytical solution of the ideal linear model of SMB and discussed it in the case of a four-column system [19]. This solution can be extended to any number of columns in each section (not necessarily the same number in each section). This solution allows the exact calculation of the concentration profiles along the columns and of the concentration histories at the extract and raffinate ports during the start-up operation and under steady-state conditions. It can serve as a benchmark for an investigation of the influence of a finite column efficiency on the performance of the process, whether the unit has four or more columns [20,21]. It is also the starting point needed for investigations of the behavior of the SMB under non-linear conditions [22]. Finally, comparison between this exact and simple analytical solution and the results of numerical calculation allows the validation of the complex programs needed to calculate the band profiles obtained under non-ideal and/or non-linear conditions.

The present paper has two goals. First, it provides the illustrations that are needed by chromatographers to understand the basic concept of SMB separations (as opposed to its fluidic design, abundantly discussed by previous authors [1–10,14–18]) and the detailed behavior of the concentration bands of the feed components. Second, it compares the analytical solution of the linear ideal model for a simple four-column SMB (arranged in four sections of one column each) and the numerical solutions of the linear equilibrium–dispersive model obtained for the same system, with different values of column efficiency. This provides an illustration of the influence of dispersion on the band profiles and on the production and an estimate of the losses arising from the finite amount of apparent axial dispersion that takes place in all columns.

2. Theory

The description and modeling of an SMB is more complex than that of a conventional chromatographic separation. We need one model for the columns and one model for the SMB set-up. These models are described successively. We assume that the feed contains only two components. The flow-rates in the system will be chosen so that the less retained component exits at the raffinate port and the more retained one at the extract port. Because of the band spreading that takes place in non-ideal chromatography, the streams exiting at each port will not be pure.

2.1. The column model

This model is simple and quite conventional [23,24]. It includes the differential mass balance equation of the two components, their equilibrium isotherms and suitable initial and boundary conditions.

The prediction of the internal concentration profiles and of the transient changes in the extract and raffinate concentrations is based on the use of the equilibrium–dispersive model. In this model, we assume that there is an instantaneous equilibrium between the mobile and the solid phase and that the contributions to band broadening due to axial dispersion and to the mass transfer resistances can be lumped into an apparent axial dispersion coefficient, D_{ap}. The mass balance of each component in each column is written as [24]:

$$\frac{\partial C_i}{\partial t} + F\frac{\partial q_i}{\partial t} + u\frac{\partial C_i}{\partial z} = D_{ap_i}\frac{\partial^2 C_i}{\partial z^2} \quad (1)$$

where u is the linear velocity of the liquid phase in the column, F is the phase ratio ($F=(1-\epsilon)/\epsilon$, with ϵ=the total column porosity), q_i and C_i are the concentrations of component i in the solid and the liquid phase, respectively. In the ideal model, the efficiency of the columns is supposed to be infinite, the mass transfer resistances are negligibly small as is the axial dispersion. Then the coefficients, $D_{ap,i}$, are set to 0 and the right hand side of Eq. (1) becomes 0.

In non-ideal chromatography, the apparent dispersion coefficient for a column of length, L, is related to the number of theoretical plates of the column, N, by the following equation:

$$D_{ap} = \frac{u L}{2 N} = \frac{u H}{2} \quad (2)$$

where H is the column HETP. In numerous previous investigations [24–27], this model was found to be applicable to the accurate description of separations performed by liquid chromatography (notably in the case of enantiomers [24,26,27]).

Because the two phases are assumed to be in equilibrium, q_i and C_i are related through the adsorption isotherm. In this paper, we assume that the system is operated under linear conditions. Accordingly, the isotherms are given by

$$q_i = a_i C_i \tag{3}$$

where a_i is a numerical constant characterizing component i. This isotherm is non-competitive. Hence, the two examples of Eq. (1) (with $i=1$ or 2) are not coupled, the profiles of the two components do not interact. As a consequence of a linear, non-competitive isotherm, all of the concentrations in a band profile move at the same constant velocity, proportional to the slope, a_i, of the isotherm. There are no self-sharpening fronts in this case. Although it is not valid in the general case, this isotherm model is not unrealistic. For example, it accounts well for the results obtained in the separation of sugars on ion-exchange resins [17].

The conventional initial condition is a system in hydrodynamic steady-state, into which a stream of pure mobile phase is injected at the feed port and two streams of pure mobile phase are collected at the extract and raffinate ports. All initial concentrations are 0. At the initial time, the feed is substituted to the mobile phase at the feed port. During the first period, the boundary condition is that of frontal analysis in the first column, downstream of the feed port. At the end of the first period, the port positions are switched in the direction of the liquid phase, as illustrated in Fig. 1. Each column in the SMB separator is considered to be a fixed bed, except for the shift of the points of introduction and withdrawal of liquids at the end of each period. These shifts are modeled by updating the initial and boundary conditions at the beginning of each period accordingly. Therefore, the initial and boundary conditions are

$$C_i(z,0) = 0 \quad q_i(z,0) = 0$$

$$uC_i(0,t) - D_{ap,i}\frac{\partial C_i}{\partial z} = uC_i^{inl} \tag{4}$$

$$\frac{\partial C_i(L,t)}{\partial z} = 0$$

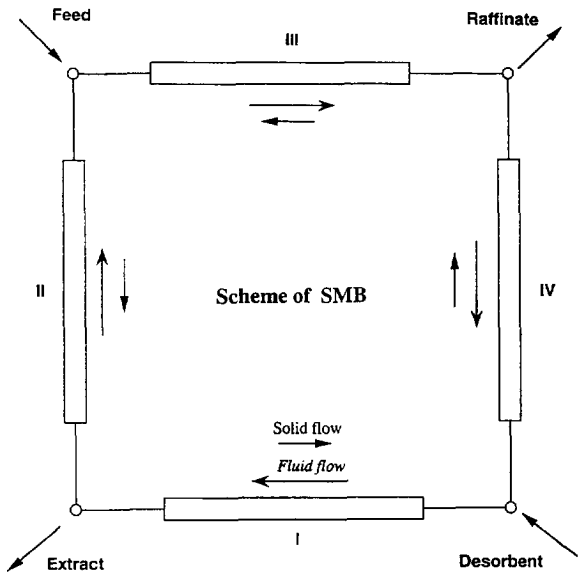

Fig. 1. Schematic diagrams of the SMB system studied. There are four pumps, one at each node. Two pumps withdraw the extract and raffinate streams. The third injects the feed. The last one injects the make-up desorbent needed to adjust its flow-rate at the inlet of column I.

where C_i^{inl} is the concentration of component I at the column inlet.

2.1.1. The SMB model

Fig. 1 gives a schematic description of the configuration of the SMB system. For the sake of simplicity, it is a four-column Sorbex system, comprising one single column per section [1,4,14,19]. Although the direction of the apparent flow of adsorbent is indicated, the operation of the SMB separator does not require any actual movement of the adsorbent. The flow of adsorbent is simulated by moving, in the direction of the liquid flow in the column series, the points of introduction and withdrawal of the liquid streams into and out of the system at a constant time interval. The separator consists of four zones, each of which consists of one or more columns. In this work, we consider only one column in each section.

The flow and mass balance conditions for the column of rank n at the beginning of a new period are the concentration profiles of the two components in the column of rank $n+1$ at the end of the previous period.

The boundary conditions at the introduction points

of the desorber and feed streams, and at the withdrawal points of the extract and raffinate streams, are written respectively as follows:

- at the withdrawal point of the raffinate stream:

$$C_{i,\mathrm{III}}^{\mathrm{ou}} = C_{i,\mathrm{IV}}^{\mathrm{inl}}$$
$$Q_{\mathrm{III}} - Q_{\mathrm{R}} = Q_{\mathrm{IV}} \quad (5)$$

- at the introduction point of the feed stream:

$$C_{i,\mathrm{II}}^{\mathrm{ou}} + Q_{\mathrm{II}} + C_{i,\mathrm{F}}Q_{\mathrm{F}} = C_{i,\mathrm{III}}^{\mathrm{inl}}Q_{\mathrm{III}}$$
$$Q_{II} + Q_{\mathrm{F}} = Q_{\mathrm{III}} \quad (6)$$

- at the withdrawal point of the extract stream:

$$C_{i,\mathrm{I}}^{\mathrm{ou}} = C_{i,\mathrm{II}}^{\mathrm{inl}} = C_{i,\mathrm{E}}$$
$$Q_{\mathrm{I}} - Q_{\mathrm{E}} = Q_{\mathrm{II}} \quad (7)$$

- at the introduction point of the desorber stream:

$$C_{i,\mathrm{IV}}^{\mathrm{ou}}Q_{\mathrm{II}} + C_{i,\mathrm{D}}Q_{\mathrm{D}} = C_{i,\mathrm{I}}^{\mathrm{inl}}Q_{\mathrm{I}}$$
$$Q_{\mathrm{IV}} + Q_{\mathrm{D}} = Q_{\mathrm{I}} \quad (8)$$

where the superscripts inl and ou refer to the inlet and outlet of the liquid stream in each zone, respectively. $C_{\mathrm{F},i}$ is the concentration of component i in the feed stream.

2.1.2. Numerical algorithms

The transient changes of the concentrations of the two components from $t = kt^*$ to $t = (k+1)t^*$, where k is an integer and t^* is the period of the SMB or its switching time, are obtained by solving numerically Eqs. (1–4) (in the equilibrium–dispersive model [24]) during the period. The profiles obtained at the end of the previous period, properly transferred from section to section in the liquid phase direction, are used as the initial condition for the calculation of the profiles during the next period. The boundary conditions (Eq. (4)) are combined with the node conditions (Eqs. (5–8)). These initial and boundary conditions are updated at the beginning of each new period. The calculation of the band profiles are made using the forward–backward finite difference method that was used with success for similar applications in many previous publications and was validated by the good agreement observed between calculated and experimental profiles [2–4,7–10,20]. An analytical solution for the linear, ideal model has been reported previously [19]. An outline of the derivation and the complete set of algebraic equations making this solution are given in Appendix A.

3. Results and discussion

The numerical calculations have been carried out with the following values of the flow-rates: $Q_{\mathrm{F}} = 0.50$ ml/min, $Q_{\mathrm{E}} = 1.286$ ml/min, $Q_{\mathrm{R}} = 0.893$ ml/min and $Q_{\mathrm{D}} = 1.679$ ml/min ($Q_{\mathrm{I}} = 4.715$; $Q_{\mathrm{II}} = 3.429$; $Q_{\mathrm{III}} = 3.929$; $Q_{\mathrm{IV}} = 3.036$ ml/min). The separation factor of the two components was supposed to be $\alpha = 2.0$. The slopes of the two linear isotherms were $a_1 = 1.0$ and $a_2 = 2.0$. The feed concentrations were $C_{\mathrm{F},1} = C_{\mathrm{F},2} = 1.0$ mM. The cycle time was $t^* = 74$ s. Under such conditions, the value of the safety coefficient, β [14,19,20], is equal to 1.2 (see values allowed for β in Table 1). It is the same for all four sections of the SMB. The efficiency of each of the four, 10 cm long, columns (assumed to have a cross-sectional area of 0.4 cm^2) was 800 theoretical plates ($F = 0.50$), except when a different efficiency was needed to illustrate some features of the profiles, when it was 100 or 3000 theoretical plates.

3.1. Concentration profiles during start-up operations in a nonideal system

In this work, we consider a simple system with only one column per section of the SMB, i.e., a total of four columns. The influence of the number of columns will be discussed later [28]. The columns are labeled accordingly as I, II, III and IV, with the feed, the raffinate and the extract ports between columns II and III, III and IV, and I and II, respectively, and the desorber being recycled from column IV into column I. The concentration profiles of the two components along the column series during the first few periods is discussed in detail. It is important to realize that, strictly speaking, the SMB process is not continuous but cyclical. During

Table 1
Allowed β values

Section	I	II	III	IV
β (Component A)	<1	>1	>1	>1
β (Component B)	<1	<1	<1	>1

each cycle, even under steady-state conditions, the spatial concentration profiles are not steady, but migrate progressively along the column series, while the concentration histories at each port are peaks or bands, not plateaus.

3.1.1. First period

The conventional initial state is a series of four columns that contain no feed components but are under hydrodynamic steady-state. At the initial time, the feed composition is raised from $C_{F,i}=0$ to its new constant state, $C_{F,1}=1$ mM and $C_{F,2}=1$ mM (these values are arbitrary but this choice is unimportant since the isotherm is linear). Accordingly, the system operates under the conditions of frontal analysis during the first period. Under linear, non-competitive conditions, the fronts of the two components migrate at a constant velocity and the profiles of these fronts are error functions [24]. The first component migrates faster than the second one and its front enters column IV before the end of the period. Under the conditions selected, the front of the second component does not enter this column. This means that, on the average, component 1 is transported faster by the liquid than by the solid phase while the converse is true for component 2. As will be made clear later, if the front of component 2 moves too fast and enters completely into this column, component 2 will not be able to move backwards far enough towards the extract port and will not be able to reach this port. The SMB will not separate the feed into two pure fractions. That does not mean that the beginning of the front, especially if it is very broad, cannot enter column IV over a short distance. In this case, a small amount of second component will exit at the raffinate port, along with the first component, and component 2 will be an impurity of the raffinate product.

The feed entering the SMB is diluted by the stream of liquid phase coming from the second section. Accordingly, the concentration of the plateaus of the two components are always lower than the feed concentrations. As derived elsewhere, this dilution factor is $1-K_A$, with $K_A=(1+FK_1\beta)/(1+FK_1/\beta)$ [19]. Fig. 2a illustrates the profiles of the two components at the end of the first period.

3.1.2. Second period

At the end of the first period, the ports are switched in the direction of the liquid stream. Accordingly, column IV becomes column III and column III becomes column II, immediately upstream of the feed inlet port. Fig. 2b shows the concentration profiles at the beginning of the second period. The feed that enters column III is now no longer diluted in a stream of pure liquid phase, but in a stream containing both components at the concentrations $(1-K_A)C_{F,i}$. The concentration plateaus which form in columns III and IV are higher than those which that these columns during the first period. Their concentrations become $(1-K_A^2)C_{F,i}$ [19]. The fronts of the two profiles move at the same velocity as before, since the velocity associated with concentration is constant.

Fig. 2c–e illustrates the profiles of the two components during (Fig. 2c–d) and at the end (Fig. 2e) of the second period. At the front and rear of each concentration plateau, steps at the intermediate

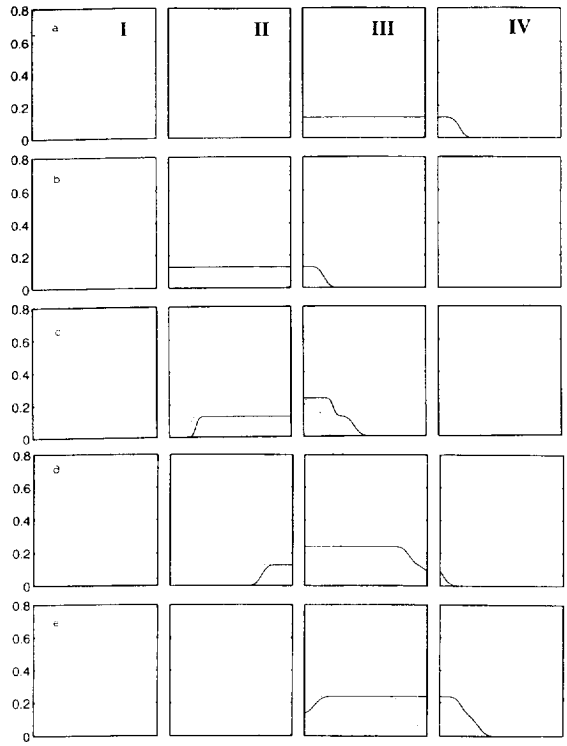

Fig. 2. Concentration profiles of the two components during the first two periods. Column efficiency, 800 theoretical plates. Solid line = first component. Dotted line = second component. Concentration profiles at (a) the end of the first period (time $t^*-\epsilon$); (b) the beginning of the second period (at time $t^*+\epsilon$); (c) time 1.2 t^*; (d) time 1.7 t^* and (e) the end of the second period (time $2t^*-\epsilon$).

concentrations $(1-K_A)C_{F,i}$ tend to form. This is because the dilution ratio of the feed in the liquid stream changes during the period. These steps can be noticed at high column efficiencies (Fig. 3a–c) but axial dispersion blurs them and disperses them into a unique front at moderate or low column efficiencies (Fig. 2c–e). The concentration profiles of the two components that are in column II at the beginning of the period move forward into column III. The plateau of the first component profile again enters into column IV stoward the end of the period and moves farther into this column than it did during the first period. A first step at a concentration of $(1-K_A)C_{F,i}$ is barely detectable at high efficiency (Fig. 3a–c). It originates from the short plateau that was in column IV at the end of the first period and was transferred into column III, hence was ahead of the

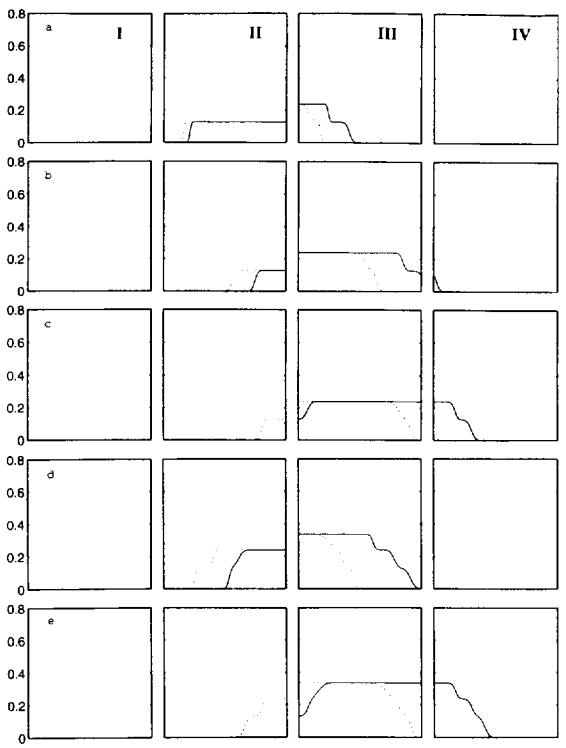

Fig. 3. Concentration profiles of the two components during the second and third periods, at high column efficiency, 3000 theoretical plates. Profiles of the first (solid lines) and second (dotted lines) components. Concentration profiles at (a) time $1.2t^*$ (cf. Fig. 2c); (b) time $1.7t^*$ (cf. Fig. 2d); (c) the end of the second period (time $2t^*-\epsilon$, cf. Fig. 2e); (d) time $2.5t^*$ (middle of the third period, cf. Fig. 4b) and (e) the end of the third period (time $3t^*-\epsilon$, cf. Fig. 4c).

feed port, at the beginning of the second period. Because the velocity of component 1 is larger than L/t^*, the part of the profile of component 1 that was in column II at the beginning of the period (Fig. 2b) has enough time to pass completely by the feed port. So, during the last part of the period, the feed is diluted again in a stream of pure liquid phase, as occurred during the first period. This explains the downward step at the end of the profile of component 1, in column III (Fig. 2e and Fig. 3c).

Similarly, since the front of the profile of component 2 did not have time to reach the end of column III during the first period, the rear of its profile in column II will not have time to exit into column III by the end of the period. A short plateau at a concentration of $(1-K_A)C_{F,2}$ will remain in this column at the end of the period, to be transferred into column I at the beginning of the third period. This takes place because the SMB operation has been designed so that the front of the profile of component 1 moves faster than L/t^* in column III, while the front of the profile of component 2 moves more slowly. Since there was little or no component 2 at the end of column II at the beginning of the period (Fig. 2b), the feed is diluted by pure mobile phase until the front of the plateau of component 2 passes the feed port and enters into column III. This explains the step at the front end of the profile of component 2 (Fig. 3a–b). This step can be seen only when the column efficiency is large enough to prevent excessive axial dispersion and the elimination of the extra inflection points.

3.1.3. Third period

The concentration profiles at the beginning of the period are shown in Fig. 4a, those at the middle and the end of this same period in Fig. 4b–c, respectively (low column efficiency). The pattern becomes clear. At the beginning of each period, the concentration profiles that had been developed progressively during the previous period take a step backwards. If profiles obtained after the same fraction of a period are compared, the front of the first component appears to be moving a little farther forward at each period during the start-up while the rear of the second component profile seems to be moving slightly farther rearward. At the same time, the maximum height of the concentration plateau in each column grows, but each time by a slightly lesser amount than

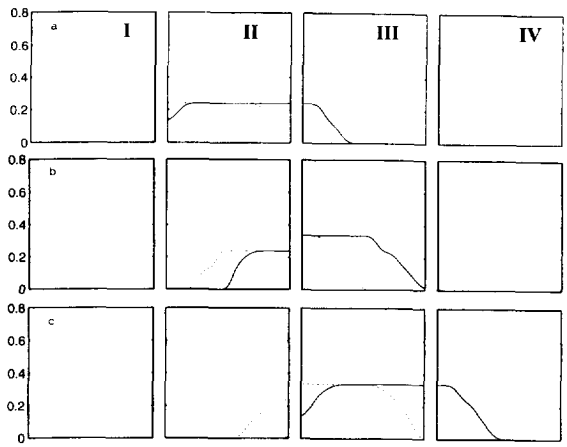

Fig. 4. Concentration profiles of the two components during the third period. Column efficiency, 800 theoretical plates. As for Fig. 2, except: concentration profiles at (a) the beginning of the third period (at time $2t^* + \epsilon$); (b) the middle of the third period (time $2.5t^*$) and (c) the end of the third period (time $3t^* - \epsilon$).

the previous one. Steps develop in a staircase at the front and rear of each profile. These steps are eroded or dispersed, most of them beyond recognition, when the column efficiency is low or moderate (Fig. 4a–c). They are more clearly visible at high column efficiency (Fig. 3d–e).

When the front of the first component profile passes the raffinate port, an aliquot of the liquid stream exits, at the same concentration. This generates a pulse of raffinate that lasts longer and contains a higher concentration of first component at each cycle. Similarly, starting with the second cycle, there is a concentration profile of component 2 that is left in column II at the end of the period. At the beginning of the following cycle, this fraction of the second component is transferred into column I. From there, it exits to column II passing by the extract port through which an aliquot exits. Thus, a pulse of extract can be collected at the beginning of each cycle starting with the third one. The amount in this pulse increases and tends towards a limit achieved when steady-state is reached. The profiles of the pulses of raffinate and extract collected during the first 40 cycles are illustrated in Fig. 5a–b. The resolution between these pulses decreases rapidly with decreasing column efficiency. Under the experimental conditions selected, the column efficiency is sufficient to achieve nearly total separation. Although a pulse of both components is found in each of the two product streams, the amount of component 2 in the raffinate and of component 1 in the extract are negligible. The influence of column efficiency on the product purity is discussed later.

3.1.4. Fourth to tenth periods

The pattern already noted is confirmed. The band profiles at the end of each period are illustrated in Fig. 6a (fourth period) to Fig. 6f (ninth period) under conditions of lower efficiency. The changes observed are minimal. The position of the front of the profiles of component 1 in column IV and of component 2 in column III tend towards limits that are located close to the exits of the respective columns, without quite reaching them. Similarly, the rear boundaries of the profiles of component 1 in column II and of component 2 in column I tend towards limits that are close to the respective inlets of these columns, but do not reach them under the conditions selected. Finally, the maximum concentration of each profile increases at each period, tending towards a limit.

The concentration plateaus of component 2 in column II and component 1 in column III have nearly reached their respective steady-state heights by the end of the seventh period. At the lower efficiency (Fig. 6a–f), the concentration profiles are round-shaped and exhibit no ripples around their top, nor steps on their front or rear (e.g., Fig. 6f). At higher efficiencies (profiles not shown), some such ripples become noticeable, but it is only at very high efficiencies that they would become significant [20]. A more sensitive test of steady-state, the area under the profile of each concentration pulse in the extract and raffinate streams, shows that steady-state is achieved only around the thirtieth period or slightly beyond. This will be discussed later.

3.1.5. Steady state

By definition, the concentration profiles in the SMB under steady-state conditions are given by an asymptotic solution and no such solutions are available under analytical, closed form for the SMB boundary conditions in the non-ideal case. However, the analytical solution obtained for each step in the ideal, linear case gives also an asymptotic solution that is obtained by using the classical results regarding infinite suites, series and products [19]. This

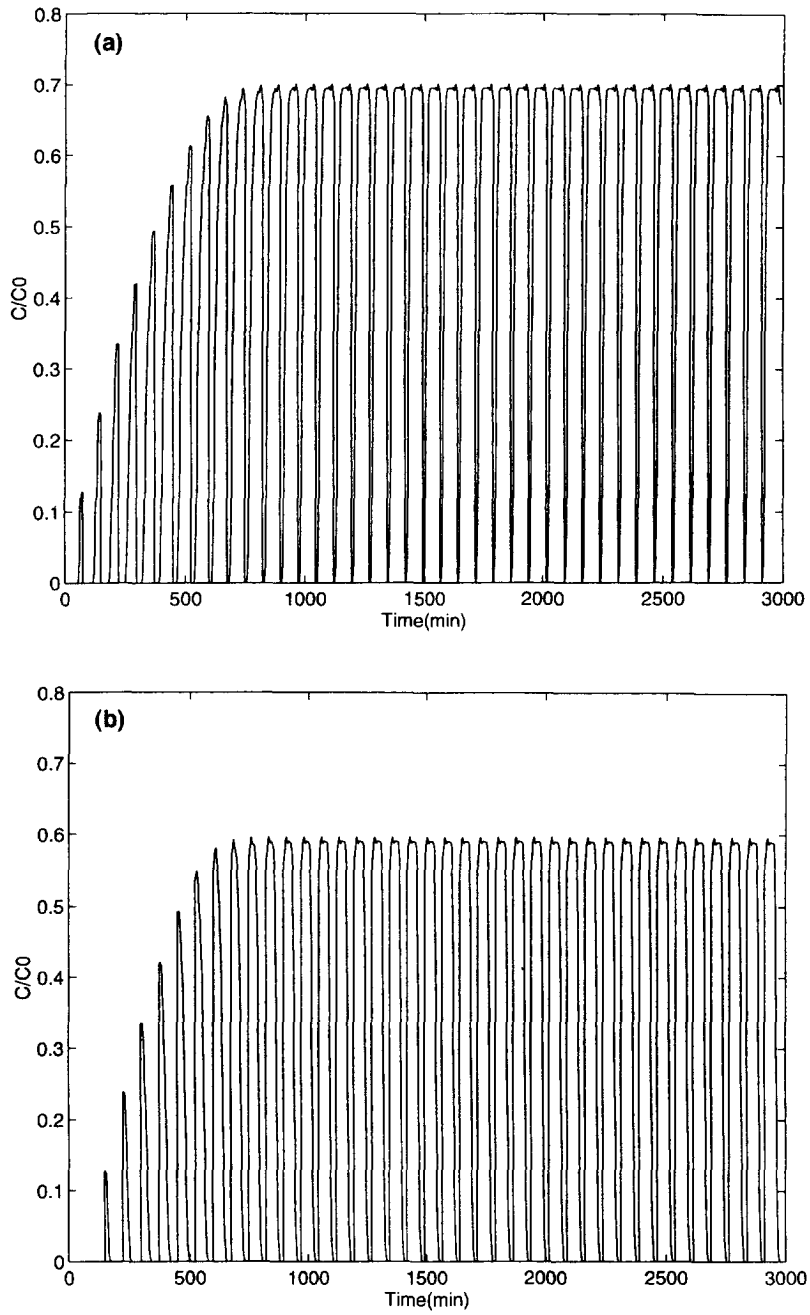

Fig. 5. Concentration histories of the outputs of the SMB. Efficiency of each column, 800 theoretical plates. This efficiency is insufficient to achieve complete separation under the conditions selected. Profiles of the pulses of (a) component 1 in the raffinate collected during the first 50 cycles and (b) component 2 in the extract collected during the first 50 cycles.

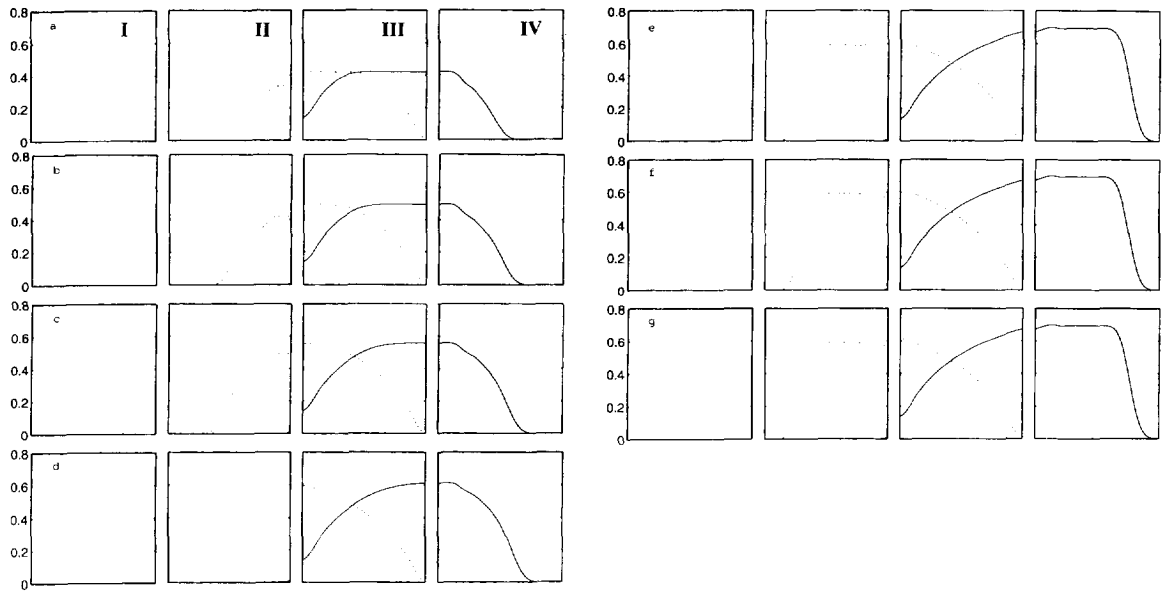

Fig. 6. Concentration profiles at the end of the different periods during start-up. Column efficiency, 800 theoretical plates. Concentration profiles at the end of (a) the fourth period (time $4t^* - \epsilon$); (b) the fifth period (time $5t^* - \epsilon$); (c) the sixth period (time $6t^* - \epsilon$); (d) the seventh period (time $7t^* - \epsilon$); (e) the tenth period (time $10t^* - \epsilon$); (f) the twentieth period (time $20t^* - \epsilon$); (g) the 30th period (time $30t^* - \epsilon$) and (h) the 35th period (time $35t^* - \epsilon$).

solution can be used to define the distance from steady-state conditions at the end of each cycle. The concentration profiles of the two components do not vary much from cycle to cycle after the thirtieth cycle. The differences become smaller than can be seen in a published figure. This is illustrated in Fig. 6g–h, which shows the concentration profiles at the end of the thirtieth and thirty-fifth cycles, respectively. It is more informative to compare the results obtained with the analytical solution of the linear, ideal model and with the numerical solution of the non-ideal model for different values of column efficiency.

3.2. Comparison between the results of the analytical and the numerical solutions

The analytical solution of the ideal model describes exactly the concentration profiles at any time during any cycle and the profiles of the pulses of extract and raffinate produced during each cycle [19]. This solution also gives these profiles for the asymptotic solution, i.e., under steady-state conditions. It is important to compare the main features of this analytical solution and their evolution from cycle to cycle with the results obtained by calculation of the numerical solutions.

3.3. Production of extract and raffinate

Fig. 7a–b shows plots of the amount of raffinate and extract, respectively, that are produced during each cycle versus the cycle rank. The calculations were carried out for columns having an infinite efficiency (analytical solution of the ideal, linear model) and for columns having 3000, 800 and 100 theoretical plates. For a given value of the feed flow-rate, the amounts of both products obtained during each cycle under steady-state conditions are independent of the column efficiency. The mass balance of the SMB demands that, under steady-state conditions, the average mass flow-rate of each compound going into the unit be equal to the average mass flow-rate going out. However, the products collected under steady state are not necessarily pure. For example, under the experimental conditions

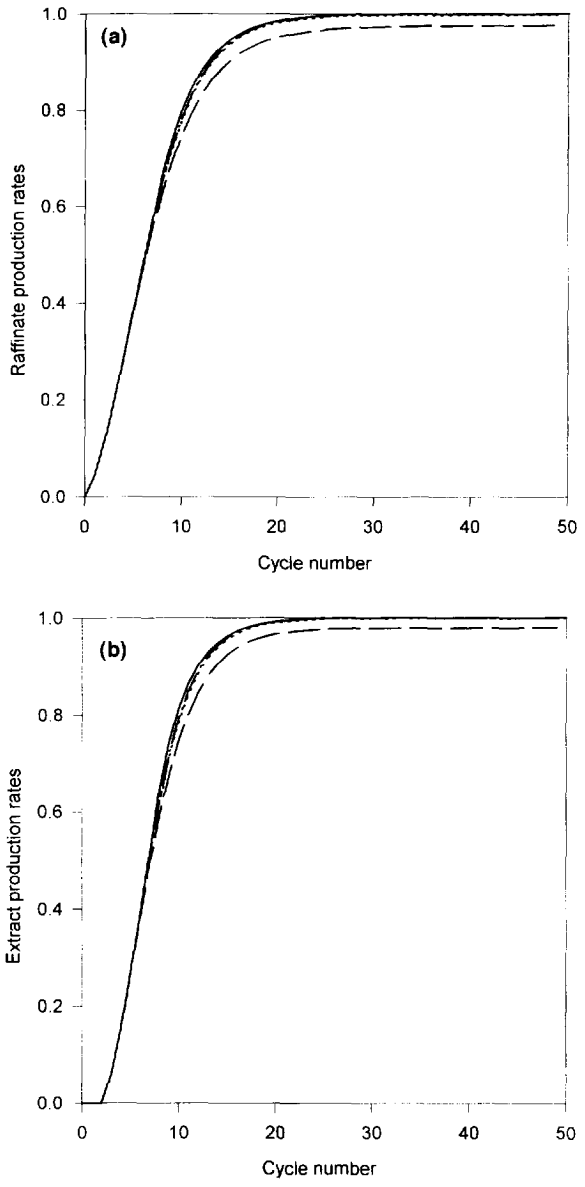

Fig. 7. Normalized productions of raffinate and extract during the start-up operation of the SMB (first 50 periods). Comparison between the values derived from the analytical solution and the values calculated for columns of finite efficiency. Column efficiency: dashed lines, 100 theoretical plates; dotted line, 800 theoretical plates; dash-dotted line, 3000 theoretical plates; solid line, infinite column efficiency (analytical solution of the ideal, linear model). Plots of the area of each pulse divided by the area of the pulse under steady-state conditions in the ideal model versus the cycle rank are shown. (a) Production of raffinate. (b) Production of extract.

selected here, the purity is perfect for infinitely efficient columns (ideal model), better than 1 ppm for $N=3000$ theoretical plates and still very high for $N=800$ plates. It is approximately 2.8% for the extract and 1% for the raffinate with $N=100$ plates. This explains why the three lines corresponding to the three highest efficiencies tend towards a unit production rate in Fig. 7a–b, while the fourth line ($N=100$ theoretical plates) on each figure has a slightly lower horizontal asymptote.

Fig. 7a–b shows that the production rate of each cycle during the start-up period and the reduced time or number of cycles required to reach the quasi-steady-state are practically independent of column efficiency. The demand made by the mass balance that, for each component, the mass flow-rates into and out of the unit be equal does not extend to the start-up period. A lower production-rate during this time would correspond to an excess amount of feed accumulated inside the columns, e.g., because of axial dispersion. Fig. 7a–b shows that this effect is negligibly small, even at low efficiencies. We see also in these figures that it takes approximately twenty periods in the case in point for the area of the pulses of raffinate and extract produced to become constant (exactly 22 for the raffinate and 19 for the extract). This number varies markedly with the experimental conditions [19].

Accordingly, the ratio of the amount of raffinate or extract produced during a cycle to the amount pumped into it during that period (it is constant and equal to the product $Q_F \cdot C_{F,i} \cdot t^*$) or to the amount derived from the analytical solution of the linear, ideal model for the production during a cycle under steady-state conditions (both amounts are obviously equal [19]) can be used as a convenient measure of the distance from steady-state. As shown in Fig. 7a–b, this ratio can be followed and plotted during the start-up time to determine when the process approaches steady-state operation.

The difference between the amount of feed introduced into the separator and the amounts of feed and raffinate produced is the feed inventory, which stays in the SMB during the entire campaign. This can be quite a significant amount. Integration of the curves in Fig. 7a–b shows that it is of the same order of magnitude as the amount of feed introduced during a dozen periods. This becomes negligible only when

the production campaign involves a large number of periods. The inventory can be recovered at the end of the campaign, albeit at a low concentration.

3.4. Concentration profiles of the two components in the SMB

Fig. 8a–e compares two sets of concentration profiles along the column calculated at the end of the first, second, third, ninth and twentieth periods, respectively. The calculations have been performed using the numerical solution of the equilibrium–dispersive model with 800 theoretical plates and the analytical solution of the ideal, linear model [19]. There is excellent agreement between these profiles, except for the axial dispersion resulting from the finite column efficiency.

The frontal discontinuity in the profiles of the two components observed in Fig. 8a in the case of the ideal model is replaced by an error function with a variance that is proportional to the column HETP and to its length in the case of the non-ideal model. All of the intermediate steps that arise in the analytical solution of the ideal linear model, because of the cyclical operation of the SMB, are similarly dispersed (Fig. 8b–f). The intensity of this axial dispersion and its effect on the profiles depends on the columns' efficiency. When column efficiency is low or moderate, the different steps are so strongly dispersed that the various steps are merged into one single dispersed boundary, as shown in Fig. 8b–e. When the column efficiency is high, some intermediate inflection points subsist in the profiles of the disperse boundaries, corresponding to some steps in the ideal profile (Fig. 8f calculated with $N=3000$ theoretical plates).

For an actual SMB, when the number of periods is small, the concentration plateaus of component 1 in column III and of component 2 in column II are flat and relatively long, compared with the column length. When the number of periods increases beyond the first few ones, the widths of the concentration plateaus of the two components decrease and tend towards zero. With 800 theoretical plate columns, these plateaus disappear for component 2 beyond the seventh period and for component 1 beyond the ninth period. These numbers are larger for more efficient columns and are lower for less efficient ones. The concentration profiles of the steady-state are round and featureless (Fig. 6g Fig. 8e–f). Compared to the staircase profiles of the ideal linear model (Fig. 8f), they are slightly shifted towards the opposite direction to that of desorber flow.

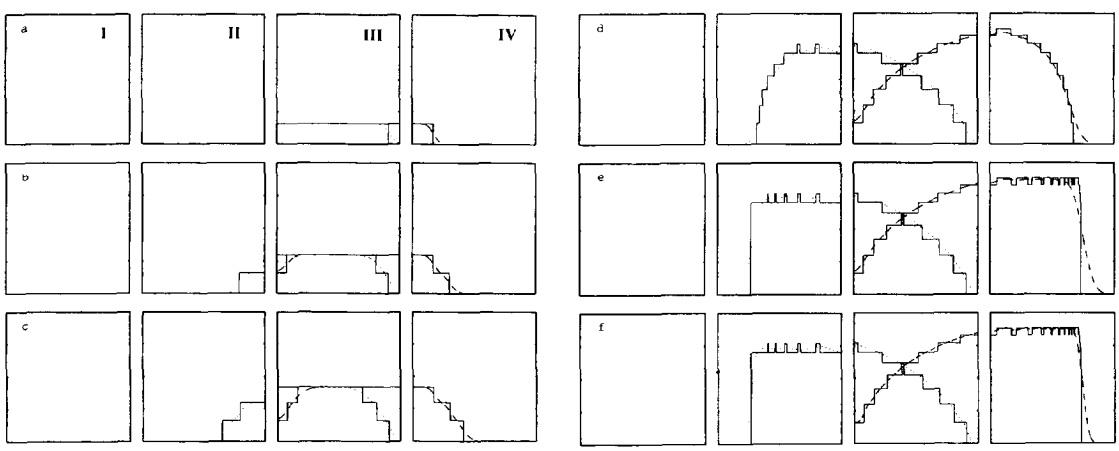

Fig. 8. Comparison between the concentration profiles of the two components given by the ideal linear model (solid lines in staircases, as in Fig. 9) and those calculated for columns having a finite efficiency (dashed line for component 1, the raffinate, and a dotted line for component 2, the extract). Column efficiency, 800 theoretical plates for (a)–(e) and 3000 plates for (f). Profiles at the end of (a) the first period (time $t^*-\epsilon$); (b) the second period (time $2t^*-\epsilon$); (c) the third period (time $3t^*-\epsilon$); (d) the ninth period (time $9t^*-\epsilon$); (e) the twentieth period (time $20t^*-\epsilon$) and (f) the twentieth period (time $20t^*-\epsilon$), with a column efficiency of 3000 plates.

3.5. Distance from steady-state

Fig. 7a–b illustrates the progressive drift of the SMB production towards steady-state conditions. They show that, in practice, the distance from steady-state conditions is independent of the column's efficiency. It is a function of the period rank and probably of some of the experimental conditions. The analytical solution developed earlier [19] offers a way to characterize quantitatively the distance from steady-state. In this work, the migration distance of the front of component 1, at the end of the nth period, in its concentration profile along column IV, Λ_n^a, is one of the characteristics of the profile of component 1 that is easy to calculate. The migration distance of the rear of component 2 in its concentration profile along column II, Λ_n^d, is one of the characteristics of the profile of component 2 that is also easy to calculate. These distances are given by the following equations

$$\Lambda_n^a = L_0^a + L_1^a + ... + L_{n-1}^a = \frac{1 - K_B^n}{1 - K_B} L_0^a$$
$$= (1 - K_B^n)\Lambda_\infty^a$$

$$\Lambda_n^d = L_0^d + L_1^d + ... + L_{n-1}^d = \frac{1 - K_C^n}{1 - K_C} L_0^d$$
$$= (1 - K_C^n)\Lambda_\infty^d$$

where L_0^a is the migration distance of the front of component 1 in column IV at the end of the first period, L_0^d is the migration distance of the rear of component 2 at the end of the second period, n is the period rank, Λ_∞^a and Λ_∞^d are the migration distances under steady-state conditions (i.e., in the asymptotic solution) and the expressions K_B and K_C are given by

$$K_B = \frac{1 + F_{a_1}/\beta}{1 + F_{a_2}/\beta} \quad (9a)$$

$$K_C = \frac{1 + F_{a_1}\beta}{1 + F_{a_2}\beta} \quad (9b)$$

In the case in point, K_B and K_C are equal to 0.7727 and 0.7273, respectively.

The rank of the period at the end of which the migration distances of the front of the profile of component 1 in column IV and at the rear of the profile of component 2 in column II are equal to 0.99 times the asymptotic value can be safely taken to be the period at which steady-state is reached. We obtain two different values (and should take the larger one):

$$n = \frac{-2}{\log K_B} \quad (10a)$$

$$n = \frac{-2}{\log K_C} \quad (10b)$$

Combination of Eqs. (9) and (10) gives the value of n, which is a function of F, a_1, a_2, and β. Because of the logarithmic dependence of n on K_B and K_C, we cannot anticipate a wide variation of n with the experimental conditions. The solution of these two equations for the set of experimental conditions used in the calculations, the results of which were reported and discussed earlier, give $n = 18$ for the raffinate and $n = 15$ for the extract. Comparing these values with the results of the numerical solution of the equilibrium–dispersive model of SMB reported in Fig. 7a (raffinate, $n = 22$) and in Fig. 7b (extract, $n = 19$) shows excellent agreement. To explain the slight difference between the results of Eqs. (10a) and (10b) and of Fig. 7a–b, note that the equations indicate the positions of the front shock of component 1 and of the rear of component 2 in the columns, while the figures are concerned with the amounts of raffinate and extract produced per cycle. Those are different properties of the steady-state. The positions of the end of the fronts stabilizes before their areas, as illustrated by Fig. 8d–f. Therefore, Eqs. 10a) and (10b) tend to underestimate slightly the number of periods required to reach a certain fractional level of the steady-state production rate. Nevertheless, the agreement observed is an important result that confirms the predictive value of the simple analytical solution of the ideal, linear model that we have derived previously [19].

4. Conclusion

The behavior of SMB under linear conditions is relatively simple. As explained in this work, the relationships between the experimental conditions and the performance are straightforward. Considera-

tion of the algebraic equations that express the analytical solution of the linear, ideal model allow the determination of the distance from steady-state during the start-up operations. This distance does not depend on column efficiency. As well as the number of periods required to reach a given, close approximation of steady-state operation, it is a weak function of the slopes of the linear isotherms, the phase ratio and of the safety factor, β. As we have shown, however, the purity of the products depends on the efficiency of the column. It is also a function of the safety factor. It is also important to elucidate the influence of the number of columns per section and that of the column-to-column fluctuations of the important properties such as permeability, efficiency and retention. These phenomena will be discussed in forthcoming publications [28].

5. Nomenclature

a	Slope of the linear isotherm
C	Concentration in the mobile phase (g/cm^3)
D_{ap}	Apparent dispersion coefficient (cm^2/s)
F	Phase ratio
H	Column HETP (cm)
k'	Retention factor ($k' = F \cdot a$)
L	Length of each adsorption column (cm)
N	Column efficiency
q	Amount adsorbed (g/g)
Q	Flow-rate (cm^3/s)
R	Extract recovery
t	Time (s)
t^*	Switching time interval (s)
u	Superficial velocity of liquid flow in the fixed bed (cm/s)
z	Axial distance (cm)

5.1. Greek symbols

α	Selectivity coefficient
β	Safety factor
ϵ	Total porosity of the bed

5.2. Subscripts

1	First or less retained component
2	Second or more retained component
E	Extra
F	Feed
I	Component
n	Period rank
R	Raffinate

5.3. Superscripts

inl	At column inlet
ou	At column outlet

Appendix A

Exact solution of the ideal, linear model for an SMB with four columns

The exact solution of the ideal, linear model for an SMB having four columns has been reported previously [19]. This solution is obtained by calculating the band profiles obtained at the end of each successive period, assuming no axial dispersion, an infinite rate of mass transfers and a linear isotherm. A set of recursive equations is obtained. Simple algebraic rules allow the derivation of the equation valid for steady-state. The band profiles are in the shape of two staircases, with a number of steps equal to the number of periods (up to a finite, limited number, see below). These steps have the same height on each side of the profile. The results are illustrated in Fig. 9.

Profiles at the end of step n

The height of the last (top) step of component I, built up during the nth period since start-up, is

$$C_i^n = (1 - K_A^n)C_{i,F} \tag{11}$$

(For the value of K_A, see below). Since K_A is lower than 1, the height of each successive new step decreases. The positions of the jumps from concentration 0 to C_i^1 or migration distances of these concentration steps at the end of the first period are given by

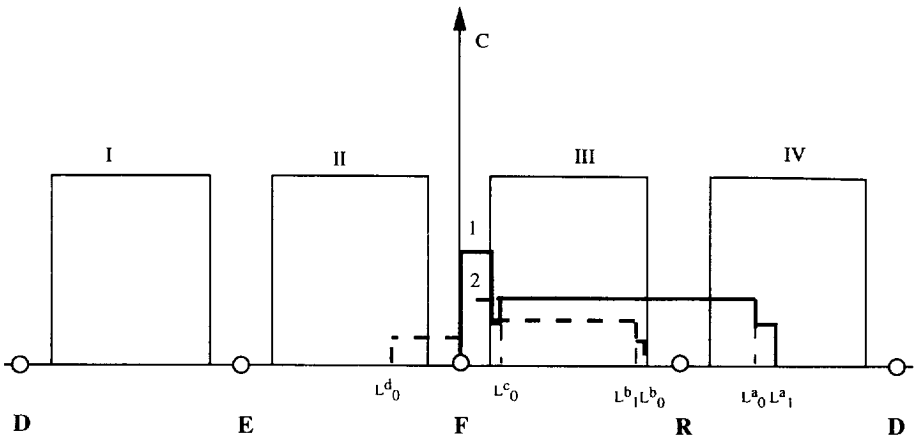

Fig. 9. Band profiles along the column calculated with the ideal, linear model. Definition of L_0^a, L_0^b, L_0^c, and L_0^d.

$$L_0^a = \frac{(\beta + k'_1)(k'_2 - \beta k'_1)}{\beta(\beta + k'_{21})(1 + k'_1)} L$$

$$L_0^b = \frac{k'_2(\beta - 1)}{\beta(1 + k_2)} L$$

$$L_0^c = \frac{k'_1(\beta + k'_2)(\beta - 1)}{\beta(1 + \beta k'_1)(1 + k'_1)} L \qquad (12)$$

$$L_0^d = \frac{k'_2 - \beta k'_1}{1 + k'_2} L$$

where the four distances L_0^a, L_0^b, L_0^c and L_0^d, illustrated in Fig. 9, correspond to the fronts of the raffinate (in column IV) and the extract (in column III), and to the rear of the raffinate (in column III) and of the extract (in column II), respectively. These distances are measured from the inlet of column IV, forward (L_0^a), from the outlet of column III, backward (L_0^b), from the inlet of column III, forward (L_0^c), and from the outlet of column II, backward (L_0^d), respectively. During the nth period, the jumps from concentration 0 to C_i^I or from C_i^I to 0 migrate forward (or backward, as applies) by the following distances (see Fig. 9), which are measured in the same direction as the former ones (Eq. (12))

$$L_n^a = K_B^n L_0^a$$

$$L_n^b = K_A^{-n} L_0^b$$

$$L_n^c = K_A^{-n} L_0^c \qquad (13)$$

$$L_n^d = K_C^n L_0^d$$

where the intermediate parameters are given by

$$K_A = \frac{Q_{II}}{Q_{III}} = \beta \frac{1 + \beta k'_1}{\beta + k'_2}$$

$$K_B = \frac{Q_{IV}}{Q_{III}} = \frac{\beta + k'_1}{\beta + k'_2} \qquad (14)$$

$$K_C = \frac{Q_{II}}{Q_I} = \frac{1 + \beta k'_1}{1 + \beta k'_2}$$

Similarly, the step between concentrations C_i^p and C_i^{p+1} (e.g., on the front of the raffinate profile, column IV) moves forward by the distance L_p^a. In other words, the migration distances of the first of these concentration steps (i.e., of the band front) at the end of the nth period are given by $\Sigma_{k=0}^n L_k^e$, with e = a, b, c or d.

Asymptotic or steady state

Because K_B and K_C are smaller than one, the corresponding distances L_n^a and L_n^d tend towards zero when n increases indefinitely. The positions of the front of the raffinate and the rear of the extract tend towards limit positions, which are given, respectively, by

$$\Lambda_\infty^a = L_0^a + L_1^a + L_2^a + \ldots + L_n^a + \ldots = \frac{L_0^a}{1 - K_B} < L$$

$$\Lambda_\infty^d = L_0^d + L_1^d + L_2^d + \ldots + L_n^d + \ldots = \frac{L_0^d}{1 - K_C} < L \qquad (15)$$

If these conditions are verified, the SMB operates properly. Otherwise, there is no purification and one of the two components seeps to the wrong port. On the other hand, the other two distances,

$$\Lambda_n^b = L_0^b + L_1^b + L_2^b + ... + L_n^b$$
$$\Lambda_n^c = L_0^c + L_1^c + L_2^c + ... + L_n^c \quad (16)$$

increase indefinitely with n. Accordingly, for certain values of n, n_R and n_E, respectively, they become equal to, or larger than, L. In this case, the concentration staircase stops and cannot be built higher. This is why only a finite number of steps is observed and the maximum concentration of the feed components in column III is always lower than their concentration in the feed.

Finally, the top of each of the two bands is flat if the corresponding length, L_n^b or L_n^c, is equal to L for a certain integer value of n. Otherwise, there is a rectangular oscillation of the concentration [19]

References

[1] D.B. Broughton, Chem. Eng. Progr., 64 (1968) 60.
[2] D.B. Broughton, R.W. Neuzil, J.M. Pharis and C.S. Brearley, Chem. Eng. Progr., 66 (1970) 70.
[3] A.J. DeRosset, R.W. Neuzil and D.J. Korous, Ind. Eng. Chem., Process Des. Dev., 15 (1976) 261.
[4] D.B. Broughton, Kirk-Othmer Encyclopedia of Chemical Technology, Vol. 1, Wiley, New York, 3rd Ed., 1978.
[5] D.B. Broughton, Sep. Sci. Technol., 19 (1984) 723.
[6] K. Hashimoto, S. Adachi, H. Noujima and H. Maruyama, J. Chem. Eng. Japan, 16 (1983) 400.
[7] K. Hashimoto, S. Adachi, Y. Shirai and M. Morishita, in G. Ganetsos and P.E. Barker (Editors), Preparative and Production Scale Chromatography, Marcel Dekker, New York, 1993, p. 273.
[8] K. Hashimoto, S. Adachi, Y. Shirai and M. Horie, J. Food Eng., 8 (1988) 187.
[9] K. Hashimoto, M. Yamada, Y. Shirai and S. Adachi, J. Chem. Eng. Japan, 20 (1987) 405.
[10] H. Maki, in G. Ganetsos and P.E. Barker (Editors), Preparative and Production Scale Chromatography, Marcel Dekker, New York, 1993, p. 359.
[11] S.C. Stintson, Chem. Eng. News, 73 (1995) 44.
[12] Anon., Chirality, 4 (1992) 338.
[13] E. Francotte, J. Chromatogr. A, 666 (1994) 565.
[14] D.M. Ruthven and C.B. Ching, Chem. Eng. Sci., 44 (1989) 1011.
[15] G. Storti, M. Mazotti, M. Moridelli and S. Carra, AIChE J., 39 (1993) 471.
[16] B.B. Fish, R.W. Carr and R. Aris, AIChE. J., 39 (1993) 1783.
[17] C.J.H. Arnold, G. Carta and C. Bayers, Ind. Eng. Chem. Res., 27 (1988) 1873.
[18] F. Charton and R.-M. Nicoud, J. Chromatogr. A, 702 (1995) 97.
[19] G. Zhong and G. Guiochon, Chem. Eng. Sci., 51 (1996) 4307.
[20] G. Zhong and G. Guiochon, Chem. Eng. Sci., in press.
[21] G. Zhong and G. Guiochon, Chem. Eng. Sci., submitted for publication.
[22] G. Zhong and G. Guiochon, Chem. Eng. Sci., submitted for publication.
[23] S. Golshan-Shirazi and G. Guiochon, in G. Guiochon and F. Dondi (Editors), NATO ASI Series, Series C, 383 (1992) p. 35.
[24] G. Guiochon, S.G. Shirazi and A.M. Katti, Fundamentals of Preparative and Nonlinear Chromatography, Academic Press, San Diego, CA, 1994.
[25] A.M. Katti, Z. Ma and G. Guiochon, AIChE J., 36 (1990) 1722.
[26] A. Seidel-Morgenstern and G. Guiochon, AIChE J., 39 (1993) 809.
[27] F. Charton, M. Bailly and G. Guiochon, J. Chromatogr. A, 687 (1994) 13.
[28] G. Zhong, T. Yun and G. Guiochon, in preparation.